Research Article

Experimental analysis on waterjet-guided Nd: YAG laser thin wood machining

Bakary S. Doumbia[1,2,3] · Chunmei Yang[1,2] · Yan Ma[2] · Qingwei Liu[1,2] · Wen Qu[1,2] · Jiuqing Liu[1,2]

Received: 11 December 2021 / Accepted: 3 May 2022
Published online: 21 May 2022

Abstract
Waterjet-Guided Laser (WJGL) machining is an advanced technique providing efficiency and precision for wood machining. The present study investigates the practical demonstration and analysis of laminated object manufacturing (LOM) WJGL for thin wood machining. A theoretical process of wood laser cutting was established, expressing relations between the cut kerf width and the influencing parameters. WJG Nd: YAG laser system was utilized for machining Korean pine and Northeast China ash specimen of 3 mm thickness, each with 7.21 and 7.13% of water content, respectively, under different machining conditions. The effects of process parameters and influences on woodcut surface geometry were analyzed via analysis of variance (ANOVA) and scanning electron microscopy (SEM). The investigated parameters include the laser cutting speed, power, kerf width, heat-affected zone (HAZ), and cut surface roughness. The study shows that the kerf width and surface were significantly influenced by WJGL power, followed by the cutting speed. For both wood specimens, at a fixed laser cutting speed of 2.36 mm/s, the kerf width increases significantly with laser power, affecting the cut surface quality accordingly. At 6 W and 8 W, the cut kerf geometry and surface quality were excellent for the *Pinus Koraiensis,* with kerf widths of 0.79 and 0.852 mm, respectively. At a fixed laser power of 8 W, the kerf width decreases with the cutting speed, affecting the cut surface quality. At a cutting speed of 4.33 mm/s, an excellent cut surface of *Fraxinus mandshurica* was observed with 0.808 mm of kerf width. Depending on the machining conditions, the kerf width variations of Korean pine were more significant than the Northeast China ash. LOM-WJGL is an efficient and eco-friendly technique for thin wood processing.

Supplementary Information The online version contains supplementary material available at https://doi.org/10.1007/s42452-022-05054-4.

✉ Bakary S. Doumbia, doumbak2017@nefu.edu.cn; ✉ Chunmei Yang, ycmnefu@126.com | [1]College of Mechanical and Electrical Engineering, Northeast Forestry University, Harbin 150040, China. [2]Forestry and Woodworking Machinery Engineering Technology Center, Northeast Forestry University, Harbin 150040, China. [3]Faculty of Sciences and Technology (FAST), University of Science Technical and Technology of Bamako (USTTB), Bamako 423, Mali.

Graphical abstract

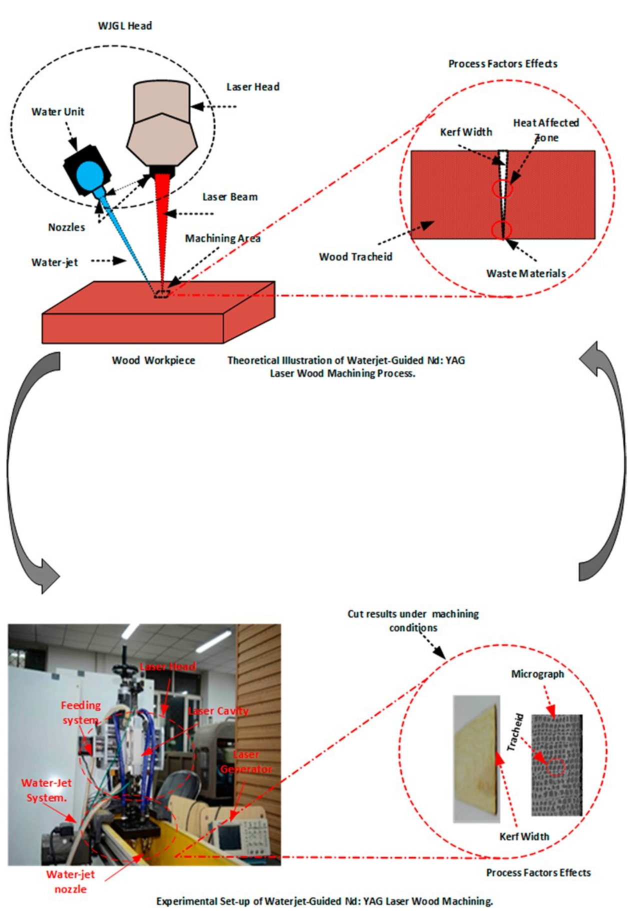

Article Highlights

- Practical modeling demonstration of waterjet guided laser (WJGL) wood machining.
- Experimental investigation of different wood specimens under influenced process parameters and machining conditions.
- Characterization and identification of suitable wood types for efficient and eco-friendly applications.

Keywords Surface geometry · Kerf width variation · Laminated object manufacturing (LOM) · Micromorphology · Waterjet-guided laser (WJGL) · Thin wood machining

1 Introduction

The recent growth of Advanced Manufacturing (AM) techniques using hybrid processes makes lasers vital, making things more straightforward and comfortable. In laminated object manufacturing (LOM), laser cutting is an applied technique with numerous lasers. The overwhelmingly used ones are conventional lasers such as carbon dioxide (CO_2), fiber/disk, neodymium-doped: yttrium–aluminum-garnet (Nd: YAG), and direct diode lasers [1–3]. The selection among these competing laser cutting systems depends mainly on the proceeded material, the efficiency (cut quality, small heat-affected zone), the flexibility of cutting regarding laser output power and cutting speed, and the process's ability to automatize [4, 5]. However, in terms of cutting objects, CO_2 and Nd: YAG lasers and derivatives are overwhelmingly used for machining a wide range of materials. They react differently with materials depending on their wavelength. The CO_2 laser is roughly 10.64 µm of wavelength, whereas the Nd: YAG laser is 1.064 µm of wavelength, which is readably ten times smaller than the CO_2 laser. Most nonmetallic materials (organic materials), including wood, are highly absorbent at the 10.6 µm wavelength of the CO_2 laser [6–8]. Whereas most metallic materials mainly absorb the short wavelength of YAG laser, it cripples its ability to absorb many other materials, including wood, acrylic, plastics, and fabrics. As a result, the Nd: YAG laser is one of the most widely used high-power solid-state lasers for high precision and micro-processing applications worldwide due to its theoretical focal point diameter [9, 10]. Consequently, its application for nonmetallic materials processing has seen considerable growth.

The pulse duration and pause duration alternate at short intervals in pulsed mode, and the laser provides pulses with high output [5, 11]. In addition, shortening the pulse width of lasers allows the surrounding area heat effects to be controlled while increasing the peak power [12]. This mode is suited for materials processing, namely, cutting, welding, and hole drilling [7, 13]. Low-powered lasers mainly use this process, resulting in a narrow, clean kerf width. Pulsed lasers are flexible systems having achieved numerous functions in optical physics. They have received special consideration in studying transient phenomena which occur in periods [14]. Overwhelmingly applied for decades to various materials, pulsed lasers have become prominent in AM technologies [5, 15]. Indeed since the 1970s, the laser has been used for wood processing as dies in the packaging industry [16]. The current application of pulsed lasers covers different types of wood materials for multiple uses, including furniture, car interiors, architecture, and indoor and outdoor decoration [5, 16–18].

In terms of thin wood laminated wooden parts machining, a certain number of studies have investigated the use of pulsed Nd: YAG solid-state lasers. Yang et al. proposed the nanosecond laser processing theory of micronized wood fibers and demonstrated the possibility of micro-thin wood fibers machining along the grain [19]. Jiang et al. used a pulsed Nd: YAG laser to cut 2 mm thick of different types of wood and study the impact of laser energy, feed rate, and kerf depth on the cut surface quality [20]. This study found significant kerf width dependency on laser pulse frequency and power. According to wood types, the increase of laser power reduced the molten slag on the wood kerf surface, improving its smoothness and quality. Bakary *et* al. currently analyzed the theoretical and practical use prospects of the pulsed Nd: YAG laser for wood veneers micromachining and found it not only eco-friendly but safe, versatile, and fast technique with less restriction resulting in a smooth cut surface with narrow kerf width without significant thermal deformation [5]. However, this study was limited to a process free of burrs and burns on the cut surface.

On the other hand, laser process efficiency in terms of versatility, eco-friendness, production capability, and in some cases, the nozzle selection and energy carriage, gas/or water-assisted laser leads to outstanding machining results [3, 5, 20–23]. Thus, WJGL is a new innovative technique that uses different laser sources assisted by waterjet for machining objects. Using the Nd: YAG laser source, WJGL technology provides high-precision operations without blurs with less heat and free debris on the cutting surface compared to conventional techniques [24]. Recently, Chunmei *et* al. have used Nd: YAG laser and waterjet guiding systems for wood laser processing to introduce a new CNC test bench for hybrid WJG Nd: YAG laser wood processing [22]. This hybrid WJGL technique is similar to the one proposed by Tangwarodomnukun et al. [25]. The process exploits the advantages of laser processing assisted off-axially by waterjet to expel debris while cooling the processed area for near thermal damage-free micromachining. Since the waterjet runs off-axially with the laser beam during processing, the distance between the two nozzles, the angle, and the waterjet offset distance, are controlled to minimize the laser beam and waterjet overlap limiting water absorption laser energy and therefore reducing heat loss. Nonetheless, heat loss at the irradiated surface may occur when the laser beam interacts with a thin water layer. The higher the power density of the laser beam energy, the greater the absorption in the water, limiting the processing efficiency of the WJGL system resulting in the slow cutting of materials [24]. As a result, different studies have been carried out using the waterjet-assisted pulsed Nd: YAG laser to cut wood parts [26, 27]. These studies analyzed the cut surface quality under the effects of process parameters and gave merit to this hybrid WJGL technique compared to conventional Nd: YAG laser cutting in terms of machining quality and efficiency.

However, considering the benefits of laser processing and, in particular, the pulsed Nd: YAG laser micromachining, plus the merit given to WJG Nd: YAG laser wood machining, there is a lack of investigations comparing the machining quality under the same conditions of different types of wood. Besides, there is no practical investigation considering the theoretical and feasibility analysis of using WJG pulsed Nd: YAG laser for wood micromachining. Therefore, besides theoretically describing the feasibility prospects, this study practically investigates using a hybrid WJG pulsed Nd: YAG laser for different thin wood micromachining under the same machining conditions. Among the two main groups of wood materials, namely, hardwood and softwood, Ash and Red pine types are selected for workpieces. These wood materials characterize hybrid WJG Nd: YAG laser thin wood micromachining. This manuscript is divided into five sections, outlined as follows. Next, we consider a theoretical analysis of laser cutting, the WJGL process, and the hybrid WJGL wood micromachining process. Section 3 shows the experimental feasibilities. In Sect. 4, the experimental findings are presented and analyzed, followed by a brief conclusion.

2 Theoretical analysis of the process

2.1 Laser cutting process

A laser cutting is a thermal process involving heating a specific workpiece material with a focused laser beam [16]. The process forms a cut kerf on the workpiece while burning or vaporizing throughout the material thickness, assisted with pressurized gas or waterjet acting co-axially to blow away the debris [7, 28]. It is a famous process used in most manufacturing industries to cut metallic and non-metallic materials [29]. Nowadays, AM technology uses competitive lasers and techniques for various applications, such as cutting, welding, and surface treatment, in schools for study and research and in small businesses. These techniques include conventional gas-assisted, remote, and non-conventional waterjet-guided laser cutting [16, 30].

Regarding the competitiveness of these techniques, the advantages of laser cutting are, among others, the precision and flexibility of contour cutting, cutting and process speed, small heat-affected zone (HAZ), cut quality, and the ability of process automatization [5, 31].

Figure 1 illustrates the process setup of conventional gas-assisted wood laser processing.

2.2 Waterjet-guided laser (WJGL)

Waterjet-guided laser technology or waterjet guided laser, also known as "Laser Micro Jet® (LMJ) presented in 1994 [32], has various applications, widely used in micromachining areas. It is a promising micromachining technique

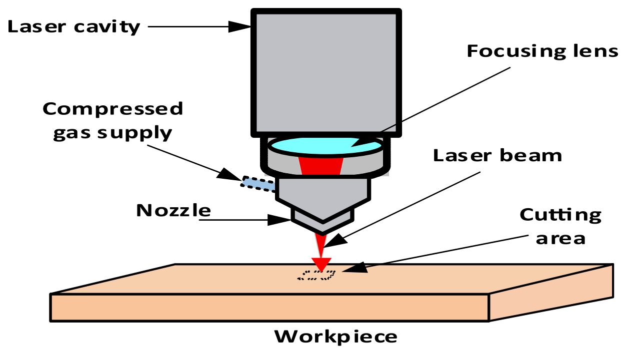

Fig. 1 Schema of classical gas-assisted laser cutting process

with many applications [33]. This laser cutting technique has been considered to have numerous advantages over conventional laser cutting techniques. These advantages include active cooling of the workpiece and material ejection, high plasma pressure, quick debris removal, and tiny focal spot size resulting in lower burrs and burns [34]. Besides, the LMJ system can operate daily in the production environment. However, new laser technologies, such as disc and fiber lasers, have been successfully applied with unique demand to various applications in the past years. Since frequency-doubled Q-switched DPSS and disc lasers operating at 532 and 515 nm have become the traditional laser sources for most LMJ applications due to their excellent compatibility with the water absorption spectrum [32]. The laser wavelength is solely constrained by the water transmission spectrum compatibility, which is minimum in the optical spectrum's green region [35]. Notably, the absorption coefficient α in the waterjet is the lowest at a wavelength of 532 nm. At 1064 nm, the absorption coefficient is about 500 times higher. Light transmission over a 2.5 cm waterjet is as high as 99.9% at 532 nm and 60% at 1064 nm [32, 35]. Hence, the light absorption at 532 nm can be neglected. Additionally, Nd: YAG laser sources with a wavelength of 1064 nm in pulsed or Q-switched regimes have also been used for water jet-guided laser systems [22, 26, 27, 32, 36].

2.3 Principle

The concept of WJGL consists of coupling a pulsed laser beam with a thin, low-pressure water jet [37]. The basic principle includes guiding the laser beam into a nozzle passing through a pressurized water chamber. The pressured waterjet cooling from the nozzle conducts the laser beam with total reflection at the water/air interface until the workpiece. Once reaching the workpiece, the guided laser beam ablates the material via the melting-vaporization process.

Depending on the nozzle diameter, the water-filled chamber has a pressure range of 50–600 bars. Larger nozzle diameters require smaller water pressure. Hence, typical nozzle diameters range from 20 to 150 µm [32]. The waterjet acts as a stable fluid optically wave guided with different lengths. Besides, it owns two other primary functions, namely [37]:

- The cooling of the workpiece cut surface, resulting in a negligible heat-affected zone (HAZ);
- The removal of excesses, molten, or debris materials from the cut kerf (heat–material interaction zone);

In other words, thin waterjet cooling prevents undesirable particles from being part of the surfaces, offering remarkable efficiency while minimizing contamination and thermal damage. Consequently, contamination and environmental risks are significantly reduced as the water jet develops high kinetic energy, efficiently removing the molten materials [32]. Furthermore, considering the small jet diameter and the low-pressured water, the waterjet's mechanical force is neglected. This force is much lower than that applied during gas-assisted laser cutting [32, 37].

2.4 Hybrid WJG Nd: YAG laser wood micromachining

Similarly, to the gas-assisted laser process (Fig. 1), for a waterjet-guided laser, the waterjet guides the laser beam during the machining process. Hence, a pulsed Nd: YAG laser of 100–500 W can be assisted by a laminar water jet to cut different kinds of materials, such as ceramics, plastics, wood, and composites, with an extraordinary degree of quality and sizeable operating stand-off distance of up to 100 mm [16]. Applying waterjet-guided solid-state Nd: YAG laser systems in thin wood product prototyping is a novel development prospect. The water jet flows co/off-axially with a laser beam through an annular nozzle. This innovative cutting process also allows continuous beams where pulsed is required. For wood machining applications, experimental studies reported that water reduces the surface roughness, decreases the kerf width, increasing the cutting speed [23, 26, 38]. Figure 2 illustrates the hybrid waterjet-guided laser wood machining. The high energy density of the assisted laser beam is focused on the wood processing region. The lignin decomposition begins at approximately 280 °C [27]. As a result, the wood cell moisture evaporated quickly, resulting in an empty tracheid. Due to a rapid temperature change, a thermal stress gradient occurs around the cutting areas. Simultaneously, local expansion and contraction occurred, resulting in micro-cracks in the wood subtract and residual stress.

Regarding wood ignition temperature, the proceeded area's laser energy density is lower than vaporization's,

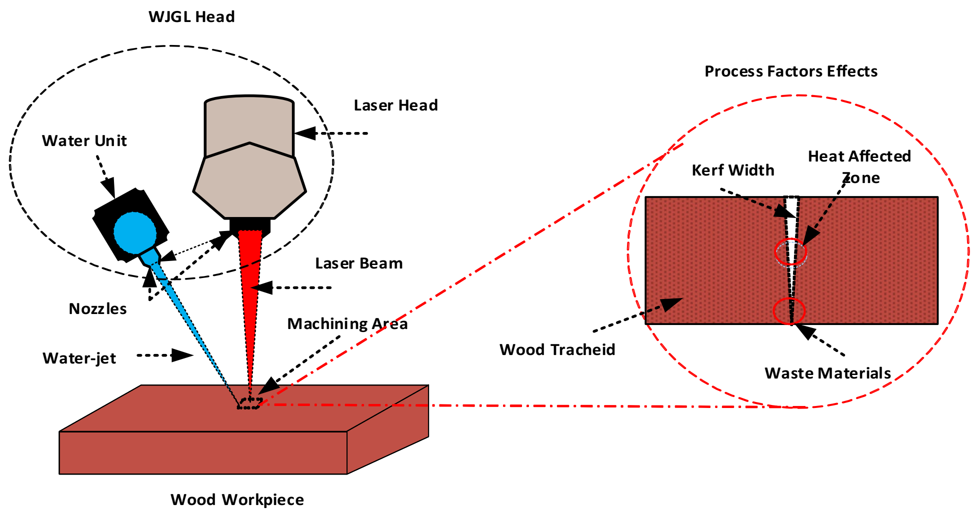

Fig. 2 Schematic illustration of hybrid WJG Nd: YAG laser wood processing mechanism

resulting in wood burning. Consequently, carbonized and heat-affected zone (HAZ) is noticeable on wood subtract surface and residues such as carbon granules and wastes, adversely affecting the cut results [23, 27, 39–41]. Therefore, the waterjet attenuates HAZ expansion, the micro-cracks. Water-cooling affects the cut kerf, cleaning away excess heat and debris and improving the WGL wood micromachining efficiency accordingly.

2.4.1 Numerical relation of influencing process parameters

Figure 3 depicts the computer numerical control (CNC) WJG Nd: YAG laser system [26]. Here, wood is fixed on the workbench, and the laser moves all along the proceeded area via the feeding system. The water moves through the nozzle outlet onto the irradiated surface when the pump is switched on, forming a jet. Simultaneously, the laser beam from Nd: YAG laser system heats up, machining the wood workpiece.

WJGL wood machining is a complex process involving multiphysics and thermal interactions. Thus, parameters of the laser system, waterjet equipment, and workpiece influence the process output. Figure 4 depicts a schematic illustration of these factors and sources based on Fig. 3.

The waterjet mechanism is additional processing of the laser process, as illustrated in Fig. 2. Water is continuously sprayed around while the laser beam is heating the workpiece. Therefore, the moisture content in processed wood is ignored. The laser wavelength and pulse width are also fixed using a pulsed laser beam. Hence, the process factors for experimental WJGL wood machining include laser

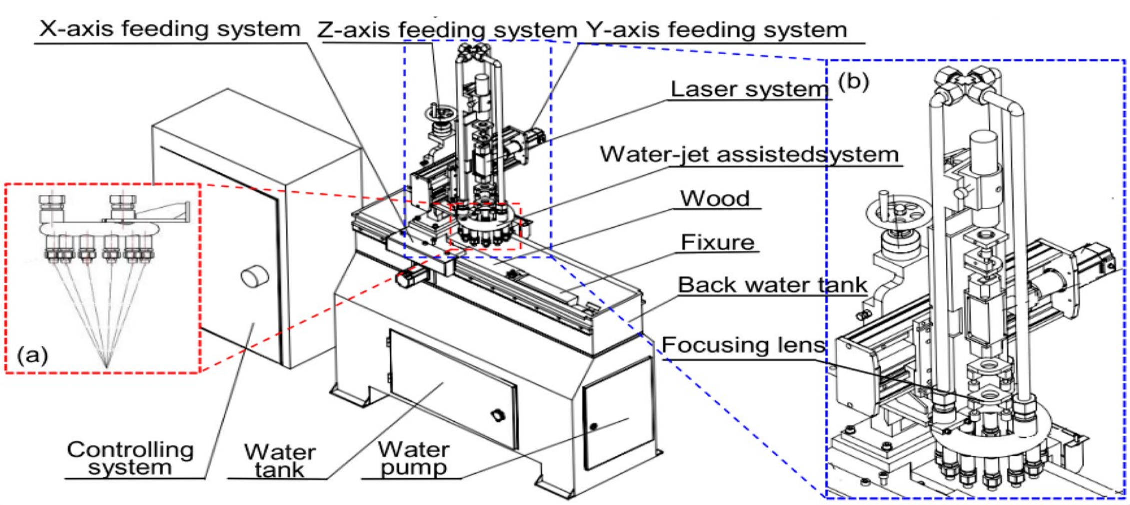

Fig. 3 Diagram of CNC WJGL processing test bench [26]. **a** Structural drawing of the nozzle, **b** structural illustration of the waterjet-guided laser system

Fig. 4 Block diagram of influencing factors of hybrid WJGL wood machining

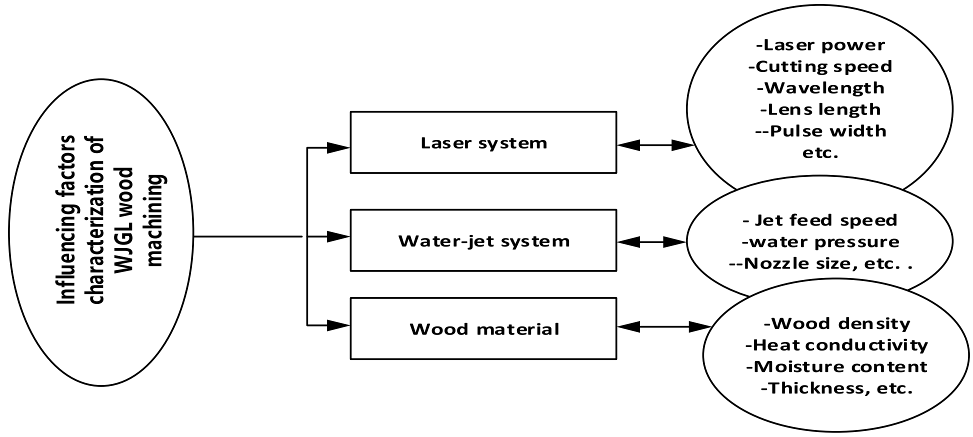

Table 1 Variables designation in Eq. (1)

Variables	Symbols & units
Laser absorbed power	P (W)
The inverse of the coupling coefficient	η
Laser incident power	P_i (W)
Wood reflectance	γ_r
Laser cutting speed	V (mm/s)
Wood thickness (Cut depth)	D (mm)
Average cut kerf width	W (mm)
Wood density	ρ (kg/m^3)
Specific heat capacity of wood	C_p (J/kg·°C)
Temperature range between wood melting and cutting	ΔT (°C)
Latent heat of wood melting	L_m (°C)
Mass of wood melted and vaporized (percentage)	M' (%)
The latent heat of wood vaporization	L_v (J/kg)

power and cutting speed, waterjet feed speed, water pressure, Nozzle outlet diameter, and wood thickness.

For pulsed Nd: YAG laser thin wood machining, the cut depth D (mm) is assimilated to the wood material thickness, which is fixed during the processing [5, 42]. As a result, laser beam energy has a remarkable influence on wood machining quality. Hence, assuming that all the absorbed laser energies melt/vaporize the wood workpiece while ignoring the heat convection and heat transfer loss, Eq. is used to express the relationship between laser power (P), cutting speed (V), and the cut kerf width (W) of processed wood material.

$$P = \eta V * W * D * \rho(C_p \Delta T + L_m + M^{'} L_v) = P_i\left(1 - \gamma_r\right) \tag{1}$$

where Table 1 reports the detail of each variable in Eq. (1).

By dividing both sides of Eq. (1) to V, one obtains Eq. (2).

$$\frac{P}{V} = \eta W * D * \rho(C_p \Delta T + L_m + M^{'} L_v) = \frac{P_i}{V}\left(1 - \gamma_r\right) \tag{2}$$

Since P_i, V, W are concerned, one got an equivalent Eq. (3), deduced by considering the right-end of Eq. (2).

$$\frac{P_i}{V} = W \times \left[\frac{\eta D * \rho(C_p \Delta T + L_m + M^{'} L_v)}{\left(1 - \gamma_r\right)}\right] \tag{3}$$

P_i is the incident laser power depending on the laser pulse energy E (m J) and pulse frequency f (Hz), expressed by Eq. (4) [5].

$$P_{\rm i} = E \times {\rm f} \tag{4}$$

Using a pulsed Nd: YAG laser with pulse energy E from 10 to 800 m J and pulse frequency f from 1 to 15 Hz, the incident laser power P_i is numerically from 0.01 to 12 W.

Since the wood workpiece thickness D and other auxiliary parameters remain fixed during the processing, Eq. (5) expresses kerf width (W) as a function of laser power (P_i) and cutting speed (V) deduced from Eq. (3).

$$W = \beta \frac{P_i}{V} \tag{5}$$

β denotes the constant part of the equation expressed by Eq. (6).

$$\beta = \left[\frac{\left(1 - \gamma_r\right)}{\eta D * \rho(C_p \Delta T + L_m + M^{'} L_v)}\right] \tag{6}$$

Notably, the kerf width (W) is proportional to the incident laser power (P_i) and inversely proportional to the cutting speed (V) at constant β.

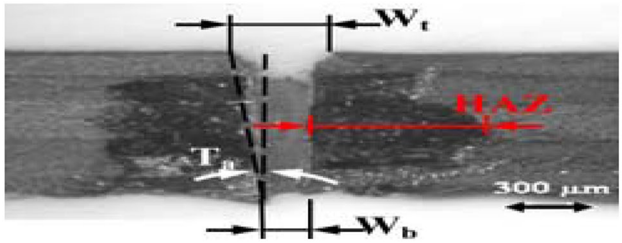

Fig. 5 Cut kerf geometry illustration [43]

Table 2 Fundamental physical characteristics of workpiece materials

Materials	Air-dry density (g/cm^3)	Moisture content (%)	Ignition point (°C)	Released heat (kJ/g)
Korean pine (*Pinus Koraiensis*)	0.45	7.21	295	19.08
Northeast China ash (*Fraxinus mandshurica*)	0.67	7.13	298	17.35

2.4.2 Cut surface geometry

The kerf geometry is one of the most factors characterizing the machining quality. Figure 5 illustrates the typical kerf geometry characterization of the laser cut surface of a solid material.

In Fig. 5, W_t, W_b, and T_a denote the top kerf width, bottom kerf width, and taper angle. The equation expresses the taper angle (T_a) function of W_t, W_b, and D [43].

$$T_a = \tan^{-1}\left(\frac{W_t - W_b}{2D}\right). \quad (7)$$

where D (mm) denotes the proceeded solid material thickness.

3 Experimental implementation

3.1 Materials and equipment

3.1.1 Workpiece materials

There are mainly two wood groups, namely, hardwood and softwood. The former is dense with significant hardness (hardwood), while the latter is soft with small hardness (softwood). Hardwood includes Ash, Chestnut, Trembling Aspen, Oak, Walnut, Beech, Palissander, Lignum Vitae, Mahogany, Teak, Abarco, Gurjun, Greenheart, Kauvula, Corkwood, Oboto, Thuja, Yellow Buckeye, etc. In comparison, softwood includes Red pine, Giant Arborvitae, Douglas Fir, Parasol Pine, Corsican Pine, Alerce, Sapwood, Dunkeld Larch, silver Fir, Pond Pine, Sugar Pine, Atlantic White Cedar, etc.

Red pine wood and Ashwood types were selected for workpiece materials, namely Korean pine, and Northeast China ash. This selection considers the difference between the two wood materials' thermophysical properties and their significance for WJGL wood machining, taking them as references and guides for further wood manufacturing. Table 2 reports the fundamental physical characteristics of the purchased wood types (Haicheng Machining Factory, Harbin, China).

The workpiece is prepared to have a specimen with a uniform thickness of 100 mm × 40 mm × 3 mm (length × width × height). Figure 6 shows the photography of the prepared samples of the two wood workpieces.

3.1.2 Equipment

A solid-state laser was selected depending on the wood laser-cutting mechanism, the thermophysical properties of proceeded material, and the test requirement vis-à-vis to the process parameters. Conventionally, wood laser cutting requires moderate laser energy. Therefore, due to its numerous advantages, versatility, and flexibility, an Nd: YAG (1064 nm) laser and auxiliary equipment (Fig. 7) were used to build the WJG Nd: YAG laser system (Fig. 8). A laser generator machine has converted electric energy into light energy (Fig. 7b). For stable laser generating, the voltage fluctuation was about three percent (3%). The cooling system used an SK20P water-cooling machine of 600 W (Dongluyang Co., Ltd., Shenzhen, China) (Fig. 7c). Table 3 shows the performance parameters of the leading equipment of the WJG Nd: YAG laser system.

3.2 Experimental processes

Referring to Fig. 3, the mechanism with a three-axis linkage feeding plate was fixed to the optical platform. The beam adjustment was carried out before installing the laser system. Firstly, while turning on the infrared tuner, the mask of the entire mirror opened and pulled down. At this moment, the tuner's spot focused on the mask's center, adjusting its height. While opening the mirror mask, it is set behind the half mirror from the entire mirror and centered, obtaining a unique, fine-tuned, coherent beam's path. The mask is placed behind the focusing lens, fine-tuned, making the beam converge with the minimum diameter after passing through the entire mirror, half mirror, and solid-state laser. Once the beam is adjusted, Nd: YAG laser is mounted with the waterjet guided equipment

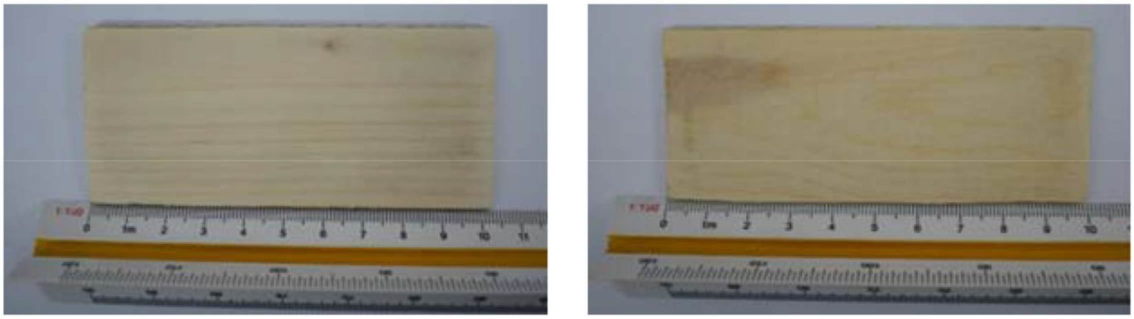

(a) (b)

Fig. 6 Test specimens **a** Northeast China ash (Fraxinus mandshurica), **b** Korean pine (Pinus Koraiensis)

(a) (b) (c)

Fig. 7 WJGL equipment [5] **a** Nd: YAG laser system, **b** Laser generator, **c** Cooling-water machine

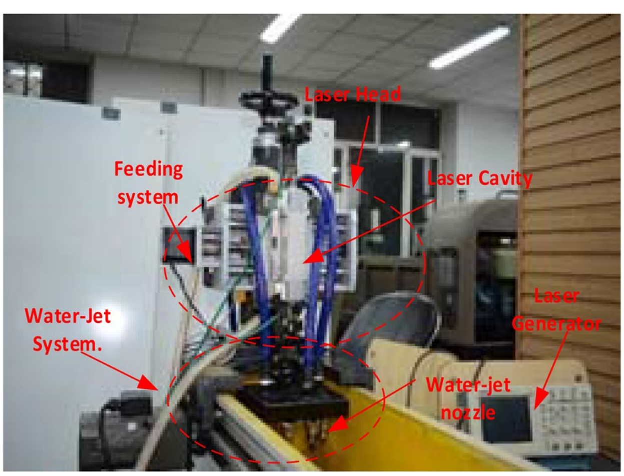

Fig. 8 Experimental set-up of WJG Nd: YAG laser wood machining

constituting the WJGL system, as shown in Fig. 8. The Gaussian (TEM00) laser beam had a 1 mm diameter and a pulse width of about 200 μs [5, 22]. The focal length of the focusing lens was 150 mm, resulting in a focus depth of 61 mm and a focal spot size of about 0.02 cm.

The workpiece is tested for an accurate operation, detecting water leakage. Depending on the waterjet cooling mechanism, an angle adjustment considers the adjustable annular nozzle to control the waterjet range for a non-overlapping with the laser beam, reducing heat loss and absorption in water. The nozzle inclination angle was adjustable to control the waterjet ring's range. The pressurized water of 0.13 MPa, flows from a nozzle outlet of 0.5 mm diameter with 5.75 m/s of waterjet speed [22, 27]. The press roller placed in the return tank is used to fix the wood on the worktable surface. Since this workpiece is

Table 3 Operating parameters of WJG Nd: YAG laser equipment

Equipment	Parameters/Variable	Specifications & units
Nd: YAG laser	Voltage (V)	220 V
	Current (A)	0–15 A
	Output power control mode	Power adjustable
	Pulse width (μs)	200 μs
	Pulse frequency (Hz)	1 ~ 15 Hz
	Pulsed voltage (V)	300 ~ 1000 V
	Pulse energy (m.J)	10 ~ 800 mJ
Cooling-water machine	Voltage (V)	220 V/50 Hz
	Refrigerant type	R134a
	Cooling flow range (L/min)	8 ~ 30 L/min
	Range of lift (m)	1 ~ 4 m
	Rated refrigerating capacity (W)	600 W

Table 4 WJG Nd: YAG laser wood machining conditions

Test conditions	Laser power (W)	Cutting speed (mm/s)	Pulse frequency (Hz)
M1	8	1.57; 2.35; 3.62; 4.68; 5.34; 6.26	15
M2	2; 4; 6; 8; 10; 12	2.36	15

M1: Korean pine and Northeast China ash specimen of 3 mm machined under experimental conditions of different laser cutting speeds of 1.57 mm/s, 3.62 mm/s, 4.68 mm/s and 6.26 mm/s, pulse frequency of 15 Hz, at a constant laser power of the water-guided laser system of 8 W

M2: Korean pine and Northeast China ash specimen of 3 mm machined under experimental conditions of different laser power of 2, 4, 6, 8, 10 and 12 W, pulse frequency of 15 Hz, at a constant laser cutting speed of the water-guided laser system of 2.36 mm/s

motionless during the processing, its position must remain unchanged, facing the system's vibration. As a result, depending on machining conditions (Table 4), the WJG Nd: YAG wood machining is adopted. By gradually adjusting the (*x, y, z*) feeding system, a test is carried out using a single pass cutting method to verify the suitability of the equipment for further subsequent processing. The wood machining was conducted once the result met the standard test requirements. Thus, Korean pine and Northeast China ash wood specimen (Fig. 6) were machined under different machining conditions, as shown in Table 4.

4 Results and discussion

Based on a theoretical model expressing the relation between process parameters, influencing factors and effects on cut surface geometry have been analyzed. An experimental test was carried out using the WJG Nd: YAG system (Fig. 8) to machine the red pine and ash wood (Fig. 6) at constant parameters and material properties (Table 2). As numerically expressed in Eq. (5), the control variable method was used to explore the relationship between the parameters. Firstly, the laser power was fixed constant while varying the cutting speed to cut the workpiece. Secondly, fixing the cutting speed, the laser power was adjusted to machine the wood workpieces as presented in Table 4. Five direct measurements of the cut kerf width were carried out using the mean value method for each selected value of laser power and cutting speed. Thus, the influence of laser power and cutting speed on cut kerf width, surface geometry, and quality are analyzed and discussed.

4.1 Influence of laser power on the cut surface (kerf width, geometry, and surface roughness)

4.1.1 Micromorphology of Korean pine cut surface under machining conditions (M_2)

Korean pine (Pinus Koraiensis) was laser cut at a constant cutting speed of 2.36 mm/s under different laser power of 2, 4, 6, 8, 10, and 12 W, pulse frequency of 15 Hz (M_2). As a result, Fig. 9 shows the machining parts and the corresponding surface micrographs of SEM. From Fig. 9, it is noticeable that the Korean pine (tube holes) lignin are approximately quadrilateral, arranged in longitudinal order. When the laser power is 4 W, the tube aperture is remarkably destroyed. The surface roughness is relatively high, presenting dross residues on the surface walls, challenging lignin visibility. At 6 W, the surface roughness is significantly improved with remarkable lignin structure, but with some remaining dross covering the tube hole. At 8 W, the cut surface is smooth, clean, visible tube aperture with no significant excess waste. Besides, the cutting quality is relatively excellent. However, when the laser

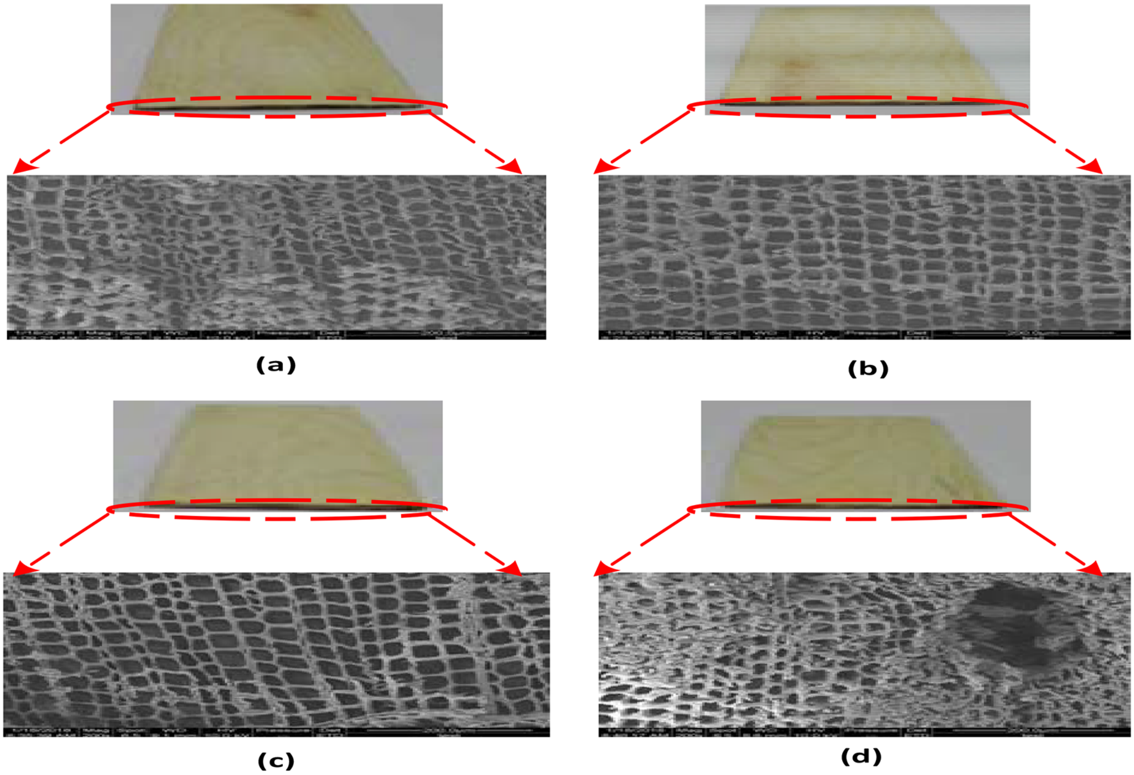

Fig. 9 Effects of laser power on the cutting surface of Korean pine (Pinus Koraiensis) **a** At 4 W, **b** At 6 W, **c** At 8 W, **d** At 10 W

Table 5 Kerf width data of Korean pine (Pinus Koraiensis) under M_2

Laser power (W)	Kerf width of Korean pine (mm)					Mean value (mm)
2	0.64	0.63	0.66	0.69	0.67	0.658
4	0.71	0.70	0.73	0.71	0.74	0.718
6	0.78	0.79	0.77	0.81	0.80	0.79
8	0.83	0.85	0.88	0.84	0.86	0.852
10	0.89	0.91	0.93	0.96	0.89	0.916
12	0.93	0.97	0.95	0.98	1.12	0.99

power is 10 W, the tube structure is destroyed, resulting in a rough surface with a significant dross presence on the cut surface.

4.2 Kerf width variations of the two wood workpieces under conditions (M_2)

Table 5 reports the kerf width data of Korean pine at fixed cutting speed for different laser power (M_2). The graph of kerf width as a function of laser power is shown in Fig. 10.

From Fig. 10, at a fixed cutting speed of 2.36 mm/s, the kerf width of the Korean pine increases linearly with the increase of the laser power, and the surface quality changes accordingly, as shown in Fig. 9. Notably, within a range of laser power, at 4 W and 12 W, respectively, for the minimum and maximum values, the surface quality of the kerf geometry is not quite good.

Similarly, Northeast China ash's specimen was machined under the same conditions (M_2) with laser power as the single variable. The kerf width data is reported in Table 6. Figure 11 shows the graphical illustration of kerf width as a function of laser power.

Figure 11 shows a remarkable variation of the Northeast China ash kerf width under different laser power, affecting the cut surface quality.

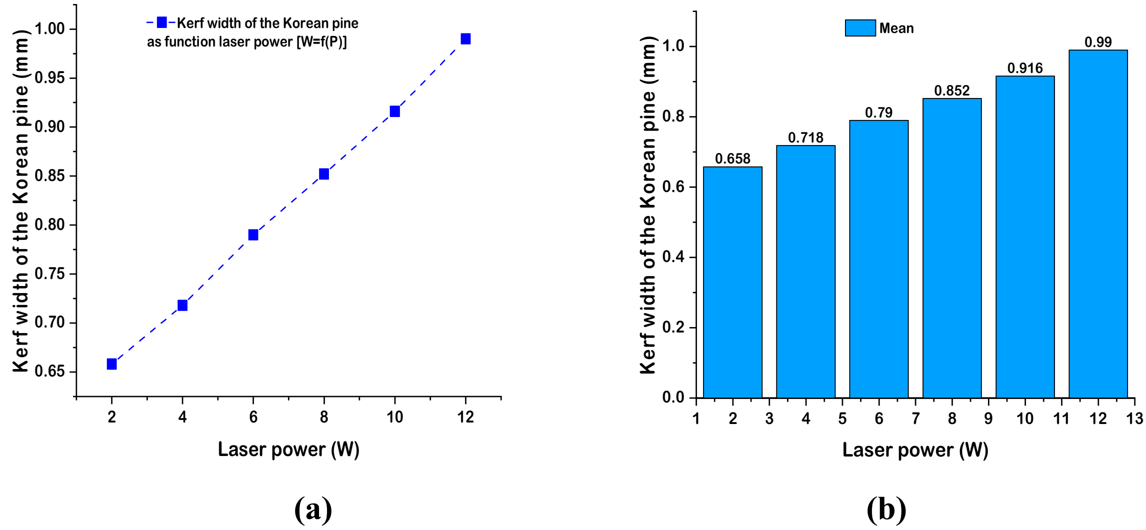

Fig. 10 Pinus Koraiensis kerf width variation as a function of laser power [$W = f(P)$] **a** Kerf width of Korean pine under different laser power, **b** Histogram of kerf width versus laser power

Table 6 Kerf width data of Northeast China ash (Fraxinus mandshurica) under M_2

Laser power (W)	Kerf width of Northeast China ash (mm)					Mean value (mm)
2	0.53	0.52	0.54	0.52	0.56	0.534
4	0.56	0.59	0.58	0.60	0.57	0.58
6	0.62	0.61	0.64	0.61	0.63	0.622
8	0.71	0.69	0.72	0.68	0.73	0.706
10	0.79	0.81	0.78	0.82	0.76	0.792
12	0.83	0.86	0.85	0.89	0.91	0.868

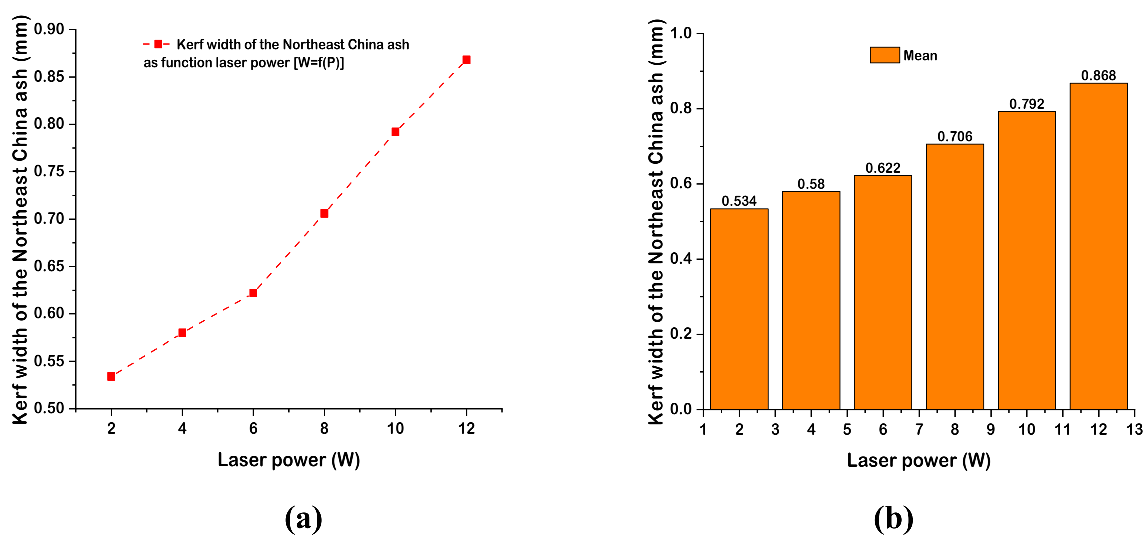

Fig. 11 Kerf width as a function of laser power of Fraxinus mandshurica [$W = f(P)$] **a** Kerf width variation of Northeast China ash, **b** Histogram of kerf width versus laser power

Table 7 Comparative kerf width data of the two wood specimens under M_2

Laser power (W)	Kerf width of the Korean pine (Pinus Koraiensis) (mm)	Kerf width data of Northeast China ash (Fraxinus mandshurica) (mm)
2	0.658	0.534
4	0.718	0.58
6	0.79	0.622
8	0.852	0.706
10	0.916	0.792
12	0.99	0.868

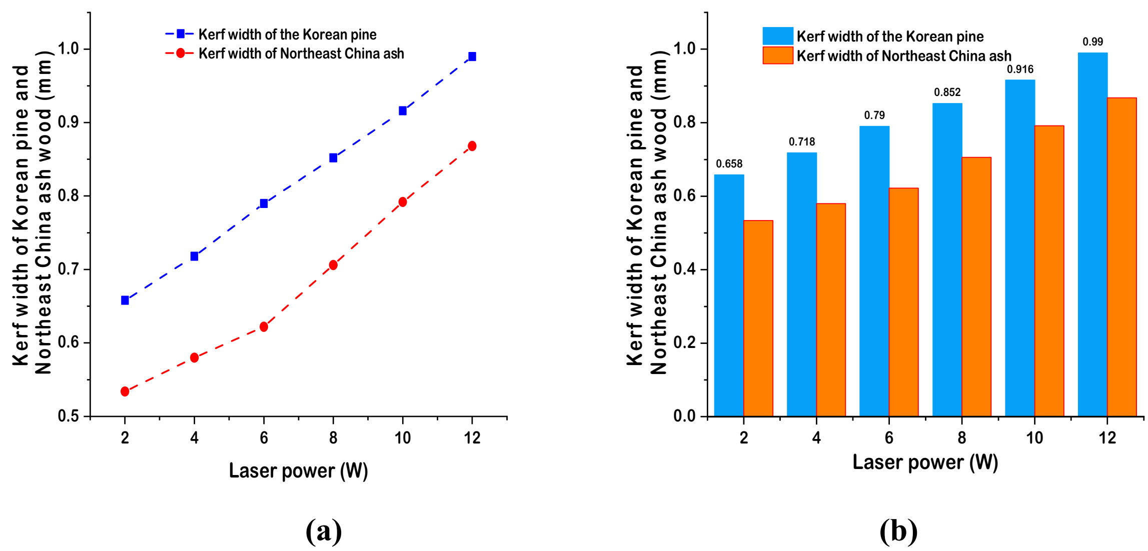

Fig. 12 Joint view of kerf width as a function of laser power of the two types of wood **a** Kerf width, **b** Histogram

From Figs. 10, 11, under M_2, the variation of laser power influence the kerf width of both Korean pine (*Pinus Koraiensis)* and Northeast China ash *(Fraxinus mandshurica)*. Under different laser power, the kerf width rises gradually, and the curve (*W* = *f (P))* slowly moves up. Consequently, the increase of the laser power leads to quick heat accumulation on the wood surface, resulting in a rapid rise in surface temperature. Under the laser beam's radiation, the wood-burning point is quickly reached. The temperature absorbed affects the kerf geometry and its surface quality accordingly.

Comparatively, under different laser power at fixed cutting speed, the kerf width variation of the Korean pine is slightly more significant than the Northeast China ash, as shown in Table 7 and Fig. 12, respectively, for kerf width data and corresponding joint graphs. This slight difference may depend on the physical properties of the two wood, as reported in Table 2. For instance, the Korean pine's air-dried wood density was lower than the Northeast China ash air-dry density. Besides, its physical properties inherent in laser energy absorption processing is quite different, resulting in the changes noticeable in Table 7.

Table 8 Descriptive statistics

	N Analysis	*N* Missing	Mean	Standard deviation	SE of Mean
P2	5	0	0.658	0.02387	0.01068
P4	5	0	0.718	0.01643	0.00735
P6	5	0	0.79	0.01581	0.00707
P8	5	0	0.852	0.01924	0.0086
P10	5	0	0.916	0.02966	0.01327
P12	5	0	0.99	0.07517	0.03362
A2	5	0	0.534	0.01673	0.00748
A4	5	0	0.58	0.01581	0.00707
A6	5	0	0.622	0.01304	0.00583
A8	5	0	0.706	0.02074	0.00927
A10	5	0	0.792	0.02387	0.01068
A12	5	0	0.868	0.03194	0.01428

Table 9 Overall ANOVA results

	DF	Sum of squares	Mean square	*F* Value	Prob > *F*
Model	11	1.08078	0.09825	110.08692	3.78944E−30
Error	48	0.04284	8.925E−4		
Total	59	1.12362			

Table 10 Fit statistics

R-Square	Coeff Var	Root MSE	Data mean
0.96187	0.03972	0.02987	0.75217

Table 11 Levine's test (Absolute deviations)

	DF	Sum of squares	Mean square	*F* Value	Prob > *F*
Model	11	0.00708	6.43758E−4	2.2402	0.02723
Error	48	0.01379	2.87367E−4		

- Analysis of variance (ANOVA)

Using the experimental data of the kerf width of the Korean pine and the Northeast China ash under condition M_2 as in appendix A [44], a One-Way ANOVA was carried out considering the WJGL power as the single independent variable. As a result, Table 8 describes the data statistics, while the ANOVA result is reported in Table 9. Table 10 shows the fit statistics of the data. The variance homogeneity was tested using Levine's (Absolute Deviations) test, as reported in Table 11.

From Table 9, in terms of the difference between the kerf width under laser power variation at a fixed cutting speed of 2.36 mm/s, the population means are significantly different at the α (0.05) level of variance. In other words, for Korean pine and Northeast China ash, there is a significant difference within the kerf widths at different laser power. Hence, laser power variation significantly influences the kerf width of the *Pinus Koraiensis* and *Fraxinus mandshurica*. Besides, the *Tukey Test* results of kerf width comparison of Korean and Northeast China ash using grouping the letter table is summarized in Table 12 (Appendix A [44]). The means that do not share a letter significantly differ at the 0.5 level. The value of Sigma (σ) was used to judge the comparison analysis. One can note that the means difference is significant at the 0.05 level of variance. Moreover, the population variance is significantly different (Table 11).

4.3 Influence of laser cutting speed on the cut surface (kerf width, geometry, and surface roughness)

4.3.1 Micromorphology of Northeast China Ash (Fraxinus Mandshurica) cut surface under machining conditions (M_1)

Fraxinus mandshurica specimen of 3 mm thick was machined under different laser cutting speeds of 1.57, 2.35, 3.62, 4.68, 5.34, and 6.26 mm/s, at a fixed laser power of 8 W. The micrographics images of SEM of the cut surface is shown in Fig. 13.

From Fig. 13, the rounded with staggered lignin wood fiber structure is noticeable along the cut surface walls. At a cutting speed of 1.57 mm/s, the cut surface is extremely rough, presenting severe ring breakage of the tube aperture with trash and crimp at the cut kerf. When the cutting speed was 3.62 mm/s, the cut surface smoothness was improved with a faintly readable tube aperture and noticeable dross on the cut kerf. At a cutting speed of 4.68 mm/s, the cut surface is smoother, flat, and relatively excellent comparatively, clean and readable lignin structure with little dross presence. While, within a selected range, at the maximum cutting speed

Table 12 The grouping letter table of the *Tukey test*

	Mean	Groups						
P12	0.99	A						
P10	0.916		B					
A12	0.868		B					
P8	0.852		B	C				
A10	0.792			C				
P6	0.79			C				
P4	0.718				D			
A8	0.706				D			
P2	0.658				D	E		
A6	0.622					E	F	
A4	0.58						F	G
A2	0.534							G

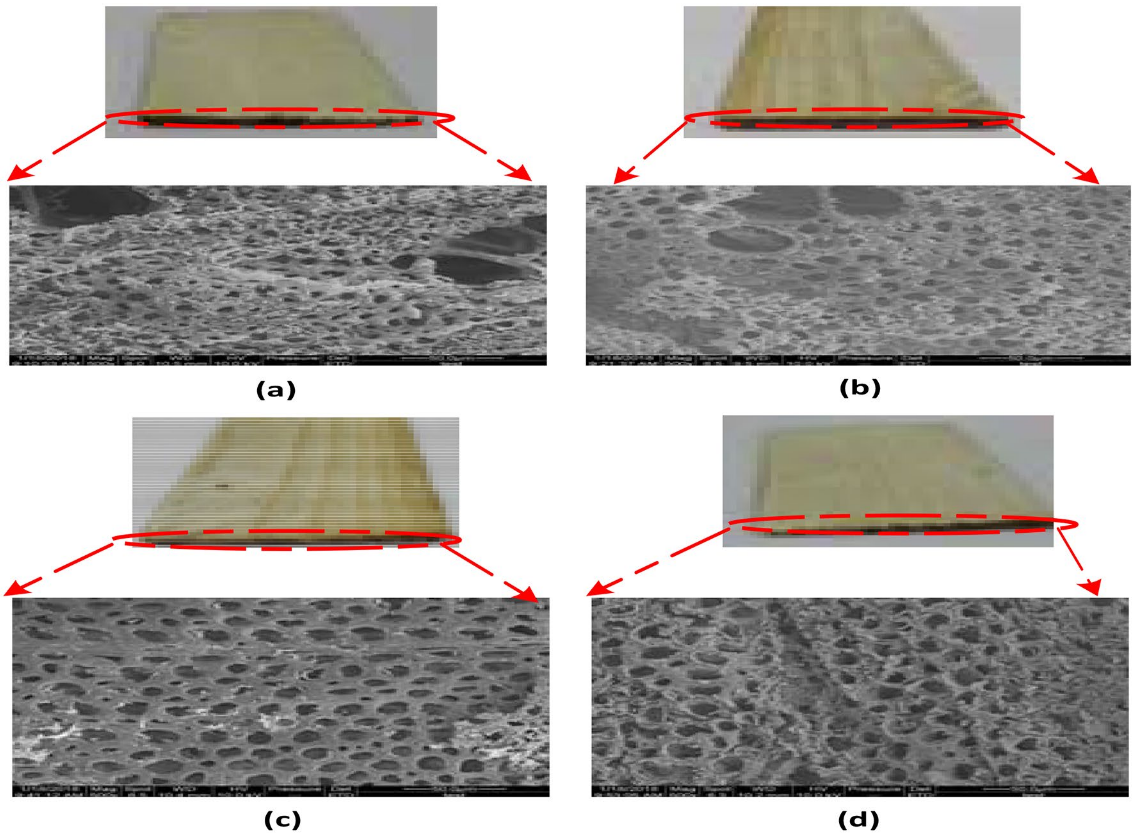

Fig. 13 Effects of cutting speed on the cutting surface of the *Fraxinus mandshurica* **a** At 1.57 mm/s, **b** At 3.62 mm/s, **c** At 4.68 mm/s, **d** At 6.26 mm/s

of 6.26 mm /s, the cut surface smoothness decreased, with an abashed lignin structure. The kerf geometry and surface quality also decreased. The surface flatness felled accordingly; it is rough with slags on the cut kerf.

4.3.2 Kerf width variations under machining conditions (M_1)

Under different cutting speeds as a single variable at a fixed laser power of 8 W, the kerf width data of the Korean pine and the corresponding variation illustration are presented in Table 13 and Fig. 14, respectively.

For Northeast China ash, the kerf width data are reported in Table 14. Figure 16 illustrates the specific variation trend.

In Figs. 14 and 15, one notices that the cutting speed variation influences remarkably the kerf widths of both types of wood specimens. For a selected wood workpiece of 3 mm thick under M_1, the increase of the WJGL cutting speed entrained the kerf width decrease, directly affecting the kerf geometry and cut surface quality accordingly, as shown in Fig. 13. Consequently, the laser beam interaction

Table 13 Kerf width data of Korean pine (*Pinus Koraiensis*) under M_1

Cutting speed (mm/s)	Kerf width of the Korean pine (mm)					Mean (mm)
1.57	0.94	0.95	0.93	0.97	1.12	0.982
2.35	0.90	0.89	0.92	0.90	0.88	0.898
3.62	0.85	0.89	0.88	0.86	0.84	0.864
4.68	0.79	0.81	0.80	0.83	0.81	0.808
5.34	0.73	0.76	0.74	0.73	0.75	0.742
6.26	0.66	0.68	0.67	0.65	0.63	0.658

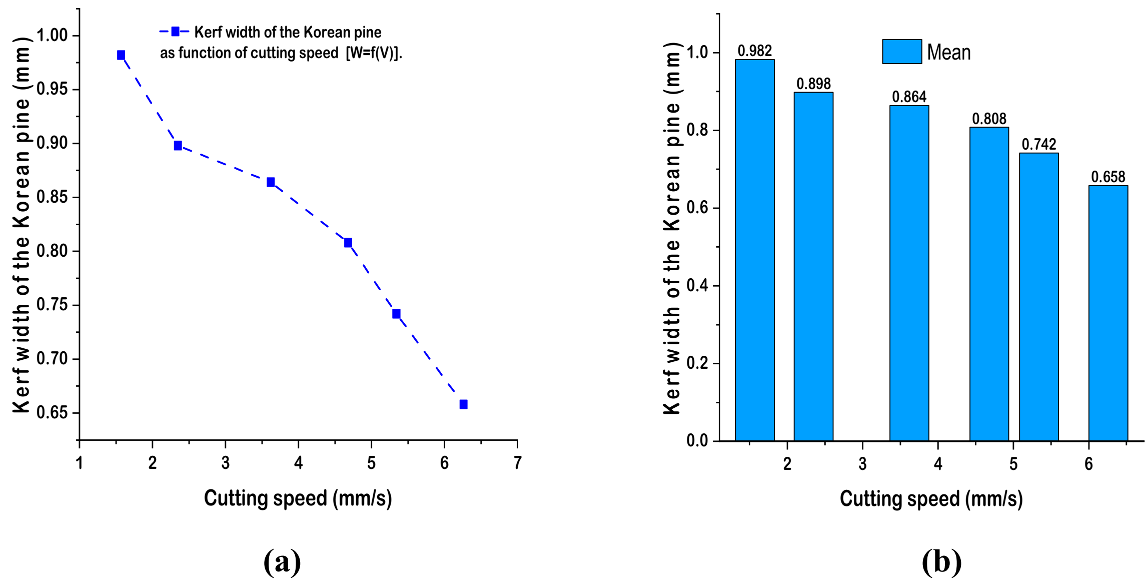

Fig. 14 Kerf width of Korean pine as a function of cutting speed [$W = f(V)$] **a** Kerf width variation of Korean pine, **b** Histogram of kerf width versus laser cutting speed

Table 14 Kerf width data of Northeast China ash (*Fraxinus mandshurica*) under M_1

Cutting speed (mm/s)	Kerf width data of Northeast China ash (mm)					Mean (mm)
1.57	0.81	0.79	0.82	0.81	0.83	0.812
2.35	0.78	0.79	0.74	0.76	0.77	0.768
3.62	0.69	0.71	0.73	0.69	0.72	0.708
4.68	0.63	0.66	0.64	0.62	0.65	0.64
5.34	0.57	0.59	0.56	0.57	0.58	0.574
6.26	0.52	0.54	0.55	0.53	0.52	0.532

with the wood is quite long at a low cutting speed. As a result, the heat accumulation time is extended, resulting in broader kerf width with a sizeable heat-affected zone (HAZ). Contrariwise, when the cutting speed increases, the interaction time is shortened. The wood-burning speed is lower than the cutting speed, resulting in a gradual decrease of the cut depth and the kerf width accordingly. However, within a range of cutting speed, at maximum cutting speed, the kerf width is thinner with dotted, serrated, little rough kerf geometry and surface (Fig. 13).

Similarly, as in M_2, under machining conditions M_1, there is a slight difference between the kerf width data of the two wood. The kerf width variation of Korean pine was still slightly more significant than the kerf width variation of Northeast China ash like in M_2, as noticed in Table 15 and graphically illustrated in Fig. 16.

- Analysis of variance (ANOVA)

Under M_1, using kerf width data of the Korean pine and Northeast China ash wood (Appendix A[44]), a One-Way ANOVA with a single independent variable of WJGL cutting speed was carried out. As a result, Table 16 shows the data statistics, and Table 17 presents the overall ANOVA summary. Table 18 reports the *Fit statistics* of the data. The variance homogeneity tested using Levine's test (Absolute Deviations) is reported in Table 19.

Considering the kerf widths of Korean pine and Northeast China ash under M_1, as shown in Table 17, the population means are significantly different at the α (0.05) level of variance. In addition, the population variances are different (Table 19). In other words, there was a significant difference within the kerf widths at different laser cutting speeds. Consequently, cutting speed affects the kerf width of the Korean pine and Northeast China ash. Furthermore, the kerf width comparison of the two workpieces using the *Tukey Test* (Appendix A [44]) summarized by the grouping letter table is reported in Table 20. The means that do not

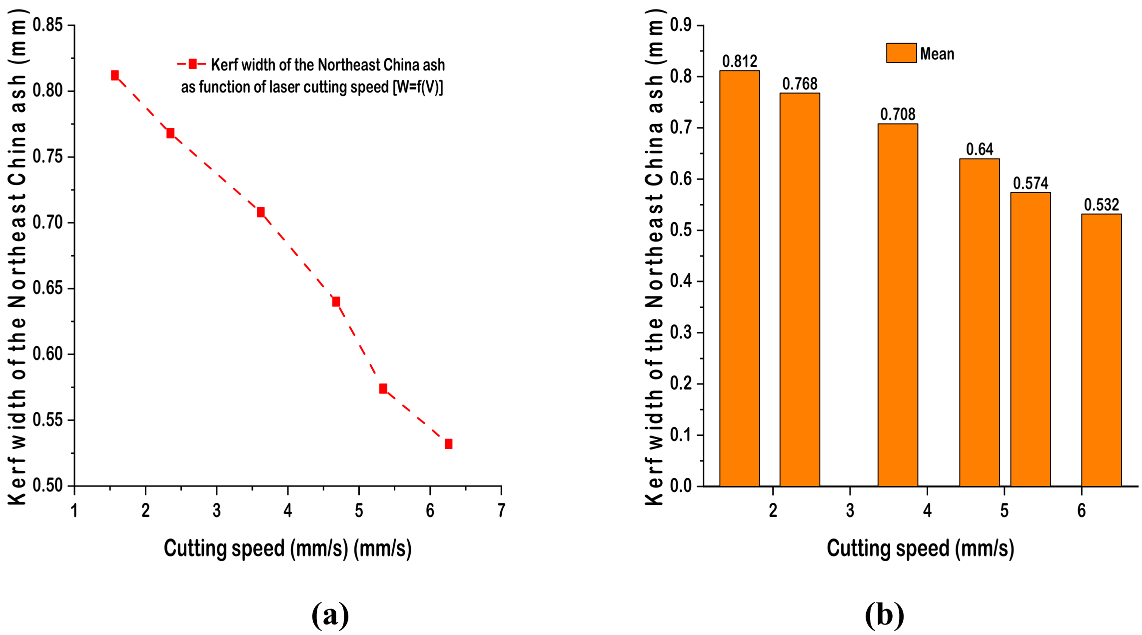

Fig. 15 Kerf width of Northeast China ash as a function of cutting speed [$W = f(V)$] **a** Kerf width variation of Northeast China ash, **b** Histogram of kerf width versus laser cutting speed

Table 15 Comparative kerf width data of the two wood workpieces under M_1

Cutting speed (mm/s)	Kerf width of the Korean pine (Pinus Koraiensis) (mm)	Kerf width data of Northeast China ash (Fraxinus Mandshurica) (mm)
1.57	0.982	0.812
2.35	0.898	0.768
3.62	0.864	0.708
4.68	0.808	0.64
5.34	0.742	0.574
6.26	0.658	0.532

share a letter are significantly different at the 0.05 level of variance.

One can note that at the 0.05 level of variance, the means difference between the Korean pine and Northeast China ash under machining conditions (M_1) is slightly significant.

4.4 Influence of the WJG laser power and cutting speed on the wood kerf width under M_1 and M_2

A two-way ANOVA with replication was conducted using Korean pine and Northeast china ash (Table 21) under M_1 and M_2 (Table 2). The data repartition in the histogram is illustrated in Fig. 17.

4.4.1 Effects on the kerf width of Korean pine (Pinus Koraiensis)

Under M_1 and M_2, a two-way ANOVA with laser power and cutting speed as independent variables influencing the Korean pine's kerf width was reported in (Appendix B [44]). The data statistic is summarized in Tables 22, Table 23, and Table 24, respectively, for laser cutting speed, laser power, and interactions. Table 25 shows the overall ANOVA result.

The kerf width comparison was evaluated using *Bonferroni Test* (Appendix B [44]). The value of Sigma (σ) judges the comparison analysis. Thus, Sig equals one (σ = 1) indicates that at a 0.05 level of variance, the difference of the means is significant, whereas Sig equals zero (σ = 0) shows that the difference is not significant. The grouping letter table of the *Bonferroni Test* summarizing the mean's comparison is reported in Table 26 and Table 27, respectively, for the cutting speed, the laser

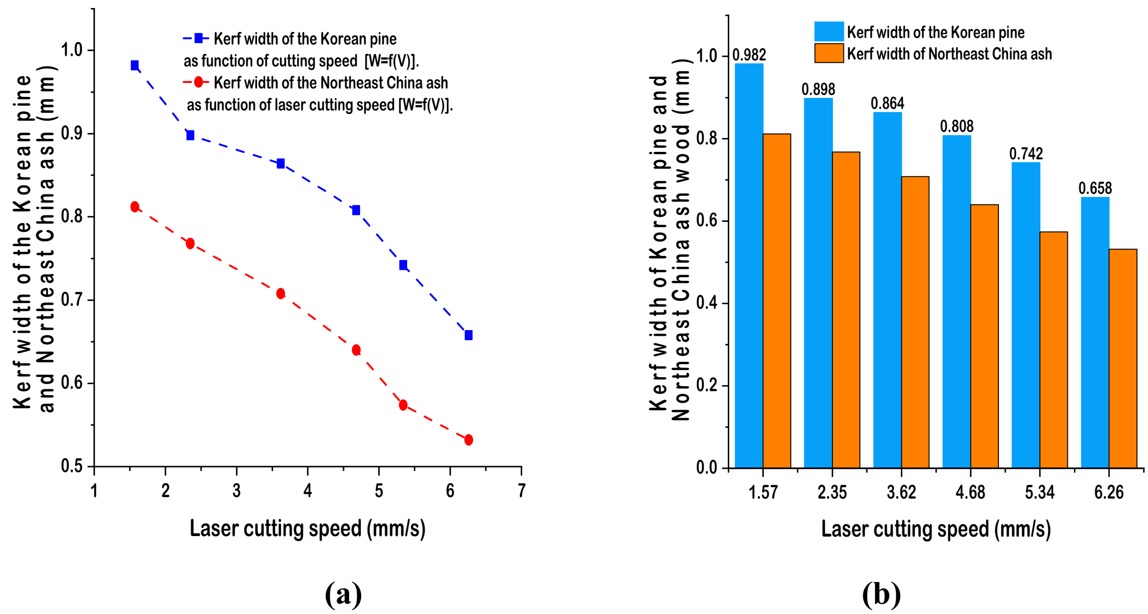

Fig. 16 Joint view of kerf width as a function of laser cutting speed of the two types of wood **a** Kerf width, **b** Histogram

Table 16 Descriptive statistics

	N Analysis	N Missing	Mean	Standard deviation	SE of mean
P1.57	5	0	0.982	0.07855	0.03513
P2.35	5	0	0.898	0.01483	0.00663
P3.62	5	0	0.864	0.02074	0.00927
P4.68	5	0	0.808	0.01483	0.00663
P5.34	5	0	0.742	0.01304	0.00583
P6.26	5	0	0.658	0.01924	0.0086
A1.57	5	0	0.812	0.01483	0.00663
A2.35	5	0	0.768	0.01924	0.0086
A3.62	5	0	0.708	0.01789	0.008
A4.68	5	0	0.64	0.01581	0.00707
A5.34	5	0	0.574	0.0114	0.0051
A6.26	5	0	0.732	0.44065	0.19706

Table 17 Overall ANOVA results

	DF	Sum of squares	Mean square	*F* Value	Prob > *F*
Model	11	0.73533	0.06685	3.95081	4.15496E−4
Error	48	0.81216	0.01692		
Total	59	1.54749			

Table 18 Fit statistics

R-square	Coeff Var	Root MSE	Data mean
0.47517	0.16992	0.13008	0.7655

Table 19 Levine's test (Absolute deviations)

	DF	Sum of squares	Mean square	*F* Value	Prob > *F*
Model	11	0.41859	0.03805	6.24738	2.89144E−6
Error	48	0.29238	0.00609		

Table 20 The grouping letter table of the *Tukey test*

	Mean	Groups		
P1.57	0.982	A		
P2.35	0.898	A	B	
P3.62	0.864	A	B	
A1.57	0.812	A	B	C
P4.68	0.808	A	B	C
A2.35	0.768	A	B	C
P5.34	0.742	A	B	C
A6.26	0.732	A	B	C
A3.62	0.708	A	B	C
P6.26	0.658		B	C
A4.68	0.64		B	C
A5.34	0.574			C

power, and their interaction. The means that do not share a letter are significantly different at the 0.05 level of variance. Figure 18 depicts the graphical illustration of the kerf width of the Korean pinewood workpiece under machining conditions M_1 and M_2.

In terms of the influences of laser power and cutting speed on the kerf width of the Korean pine, at a 0.05

Table 21 Kerf width data of the two wood specimens under M_1 and M_2

Machining parameters		Wood workpiece kerf width (mm)	
		Korean pine (Pinus Koraiensis)	Northeast China ash (Fraxinus mandshurica)
Laser power (W)	2	0.658	0.534
	4	0.718	0.58
	6	0.79	0.622
	8	0.852	0.706
	10	0.916	0.792
	12	0.99	0.868
Cutting speed (mm/s)	1.57	0.982	0.812
	2.35	0.898	0.768
	3.62	0.864	0.708
	4.68	0.808	0.64
	5.34	0.742	0.574
	6.26	0.658	0.532

level of variance, the two-way ANOVA concluded as follows:

- The population means of Cutting speed are not significantly different.
- The population means of Laser power are significantly different.
- The interaction between Cutting speed and Laser power is significant.

4.4.2 Effects on the kerf width of Northeast China ash (Fraxinus Mandshurica)

Considering the kerf width data of *Fraxinus mandshurica* under different values of laser powers and cutting speed (M_1 and M_2) (Appendix C [44]), the two-way ANOVA is statistically reported in Tables 28, 29, and 30 for laser cutting speed, power, and interaction, respectively. Table 31 reports the overall ANOVA results.

The kerf width comparison was also evaluated using *Bonferroni Test*, as reported in (Appendix C[44]). The grouping letter table summarizing the *Bonferroni Test* is reported in Tables 32 and 33 for the cutting speed, laser power, and

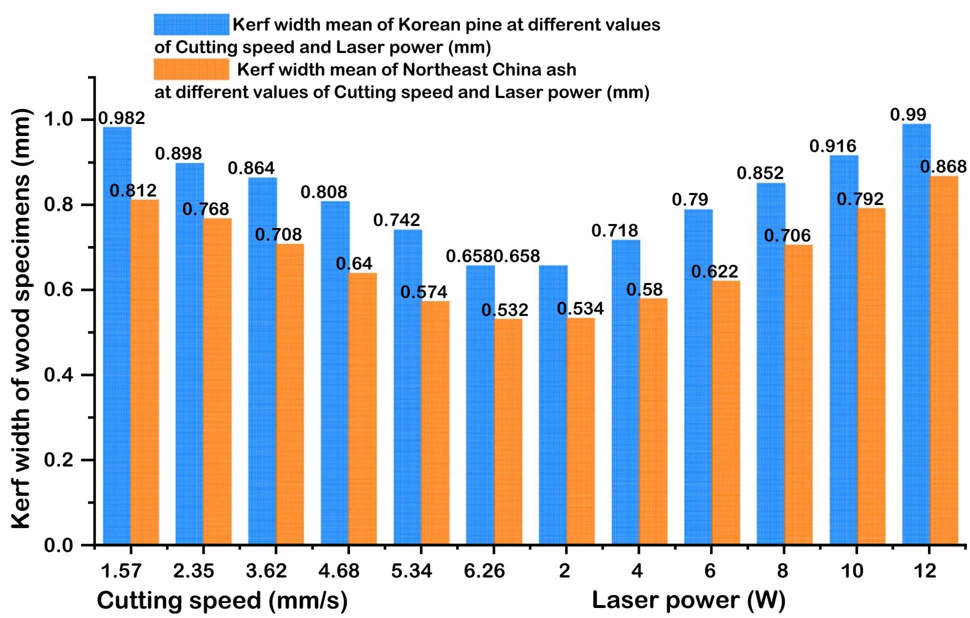

Fig. 17 Kerf width of the two wood specimens as a function of laser cutting speed and laser power

Table 22 Cutting speed

	N	Mean	SD	SEM	Variance	Missing	Non-Missing
S1.57	30	0.82067	0.11968	0.02185	0.01432	0	30
S2.35	30	0.82067	0.11968	0.02185	0.01432	0	30
S3.62	30	0.82067	0.11968	0.02185	0.01432	0	30
S4.68	30	0.82067	0.11968	0.02185	0.01432	0	30
S5.34	30	0.82067	0.11968	0.02185	0.01432	0	30
S6.26	30	0.82067	0.11968	0.02185	0.01432	0	30

Table 23 Laser power

	N	Mean	SD	SEM	Variance	Missing	Non-Missing
P2	30	0.658	0.02172	0.00397	4.71724E−4	0	30
P4	30	0.718	0.01495	0.00273	2.23448E−4	0	30
P6	30	0.79	0.01438	0.00263	2.06897E−4	0	30
P8	30	0.852	0.0175	0.00319	3.06207E−4	0	30
P10	30	0.916	0.02699	0.00493	7.28276E−4	0	30
P12	30	0.99	0.06838	0.01248	0.00468	0	30

Table 24 Cutting speed & laser power interaction

		N	Mean	SD	SEM	Variance	Missing	Non-Missing
S1.57	P2	5	0.658	0.02387	0.01068	5.7E−4	0	5
	P4	5	0.718	0.01643	0.00735	2.7E−4	0	5
	P6	5	0.79	0.01581	0.00707	2.5E−4	0	5
	P8	5	0.852	0.01924	0.0086	3.7E−4	0	5
	P10	5	0.916	0.02966	0.01327	8.8E−4	0	5
	P12	5	0.99	0.07517	0.03362	0.00565	0	5
S2.35	P2	5	0.658	0.02387	0.01068	5.7E−4	0	5
	P4	5	0.718	0.01643	0.00735	2.7E−4	0	5
	P6	5	0.79	0.01581	0.00707	2.5E−4	0	5
	P8	5	0.852	0.01924	0.0086	3.7E−4	0	5
	P10	5	0.916	0.02966	0.01327	8.8E−4	0	5
	P12	5	0.99	0.07517	0.03362	0.00565	0	5
S3.62	P2	5	0.658	0.02387	0.01068	5.7E−4	0	5
	P4	5	0.718	0.01643	0.00735	2.7E−4	0	5
	P6	5	0.79	0.01581	0.00707	2.5E−4	0	5
	P8	5	0.852	0.01924	0.0086	3.7E−4	0	5
	P10	5	0.916	0.02966	0.01327	8.8E−4	0	5
	P12	5	0.99	0.07517	0.03362	0.00565	0	5
S4.68	P2	5	0.658	0.02387	0.01068	5.7E−4	0	5
	P4	5	0.718	0.01643	0.00735	2.7E−4	0	5
	P6	5	0.79	0.01581	0.00707	2.5E−4	0	5
	P8	5	0.852	0.01924	0.0086	3.7E−4	0	5
	P10	5	0.916	0.02966	0.01327	8.8E−4	0	5
	P12	5	0.99	0.07517	0.03362	0.00565	0	5
S5.34	P2	5	0.658	0.02387	0.01068	5.7E−4	0	5
	P4	5	0.718	0.01643	0.00735	2.7E−4	0	5
	P6	5	0.79	0.01581	0.00707	2.5E−4	0	5
	P8	5	0.852	0.01924	0.0086	3.7E−4	0	5
	P10	5	0.916	0.02966	0.01327	8.8E−4	0	5
	P12	5	0.99	0.07517	0.03362	0.00565	0	5
S6.26	P2	5	0.658	0.02387	0.01068	5.7E−4	0	5
	P4	5	0.718	0.01643	0.00735	2.7E−4	0	5
	P6	5	0.79	0.01581	0.00707	2.5E−4	0	5
	P8	5	0.852	0.01924	0.0086	3.7E−4	0	5
	P10	5	0.916	0.02966	0.01327	8.8E−4	0	5
	P12	5	0.99	0.07517	0.03362	0.00565	0	5

Table 25 Overall ANOVA results

	DF	Sum of squares	Mean square	*F*-value	*P*-value
Cutting speed	5	5.55112E−17	1.11022E−17	8.33709E−15	1
Laser power	5	2.30056	0.46011	345.51589	2.66232E−78
Interaction	25	−1.38778E−16	−5.55112E−18	−4.16855E−15	–
Model	35	2.30056	0.06573	49.35941	5.7595E−64
Error	144	0.19176	0.00133		
Corrected total	179	2.49232			

Table 26 The grouping letter table of the Bonferroni Test: Cutting speed and laser power

Cutting speed (mm/s)	Mean (mm)	Groups	Laser power (W)	Mean (mm)	Groups					
S1.57	0.82067	A	P12	0.99	A					
S2.35	0.82067	A	P10	0.916		B				
S3.62	0.82067	A	P 8	0.852			C			
S4.68	0.82067	A	P6	0.79				D		
S5.34	0.82067	A	P4	0.718					E	
S6.26	0.82067	A	P2	0.658						F

their interaction. The means that do not share a letter are significantly different; elsewhere, they are not very different. Figure 19 illustrates the graphical representation of the kerf width of Northeast China ash wood workpiece under machining conditions M_1 and M_2.

Regarding the effects of the laser power and cutting speed on the Northeast China ash kerf width at 0.05 level of variance under M_1 and M_2:

- The population means of Cutting speed are significantly different.
- The population means of Laser power are significantly different.
- The interaction between Cutting speed and Laser power is not significant.

WJG Nd: YAG laser is suitable and efficient for wood machining, including softwood and hardwood. The technique provides outstanding machining results, plus it is flexible, safe, and eco-friendly [23, 26, 27]. Moreover, the waterjet reduced the surface roughness in addition to the cooling and cleaning functions; it decreased the kerf width by increasing the cutting speed due to water vaporization creating additional kinetic energy in the cutting region [23, 26, 38]. WJG Nd: YAG cutting is a suitable technique for wood machining, including thin wood from soft and hardwood. However, this hybrid WJGL processing involves multiphysics phenomena that affect irradiated surface temperature and influence machining quality. These phenomena include interaction between laser, pressurized waterjet, and air on the processed workpiece surface, which was ignored in the present study. Therefore, for further efficient and outstanding WJG Nd: YAG laser wood machining, additional studies are needed to consider the above concerns and better understand the temperature distribution (heat transfer) within the workpiece during the machining.

5 Conclusion

In this practical application of waterjet-guided Nd: YAG laser machining, the effect of influencing process parameters on cut geometry, surface, and kerf width were experimentally analyzed using the Korean pine and Northeast China ash. Based on the numerical relationship between the cut kerf width and the machining parameters, and through experimental results and analysis, the following conclusions are drawn:

1. At constant cutting speed and fixed workpiece thickness, the machining surface quality of the kerf geometry improved gradually with the increase of laser power. Excellent surface quality was obtained at the laser power of 8 W. However, with the growth of laser power, wood lignin laser beam's damage increases, decreasing the cut surface quality. Comparatively, the kerf width variation of the Korean pine was slightly more significant than the Northeast China ash.

Table 27 Cutting speed & laser power interaction

Cutting speed (mm/s)	Laser power (W)	Mean (mm)	Groups				
S6.26	P12	0.99	A				
S 5.34	P12	0.99	A				
S 4.68	P12	0.99	A				
S 3.62	P12	0.99	A				
S2.35	P12	0.99	A				
S 1.57	P12	0.99	A				
S6.26	P10	0.916	A	B			
S 5.34	P10	0.916	A	B			
S 1.57	P10	0.916	A	B			
S 4.68	P10	0.916	A	B			
S2.35	P10	0.916	A	B			
S 3.62	P10	0.916	A	B			
S 5.34	P 8	0.852		B	C		
S 3.62	P 8	0.852		B	C		
S 4.68	P 8	0.852		B	C		
S6.26	P 8	0.852		B	C		
S 1.57	P 8	0.852		B	C		
S2.35	P 8	0.852		B	C		
S 5.34	P6	0.79			C	D	
S 3.62	P6	0.79			C	D	
S6.26	P6	0.79			C	D	
S2.35	P6	0.79			C	D	
S 4.68	P6	0.79			C	D	
S 1.57	P6	0.79			C	D	
S6.26	P4	0.718				D	E
S 4.68	P4	0.718				D	E
S 3.62	P4	0.718				D	E
S 5.34	P4	0.718				D	E
S2.35	P4	0.718				D	E
S 1.57	P4	0.718				D	E
S6.26	P2	0.658					E
S 5.34	P2	0.658					E
S2.35	P2	0.658					E
S 4.68	P2	0.658					E
S 3.62	P2	0.658					E
S 1.57	P2	0.658					E

2. The cut surface quality and kerf geometry change accordingly at fixed laser power when varying the cutting speed. The increase in the cutting speed leads to a rise in the cut kerf and surface quality. However, within a chosen range, at the lowest cutting speed of 1.57 mm/s, the surface quality is relatively low. Indeed, for a constant wood property, low or high cutting speed results in lousy surface quality in a specific thickness. Comparatively, the surface quality is excellent, clean, and flat at the cutting rate of 4.68 mm/s. Besides, the kerf width difference between the Korean pine and Northeast china ash was slightly considerable.

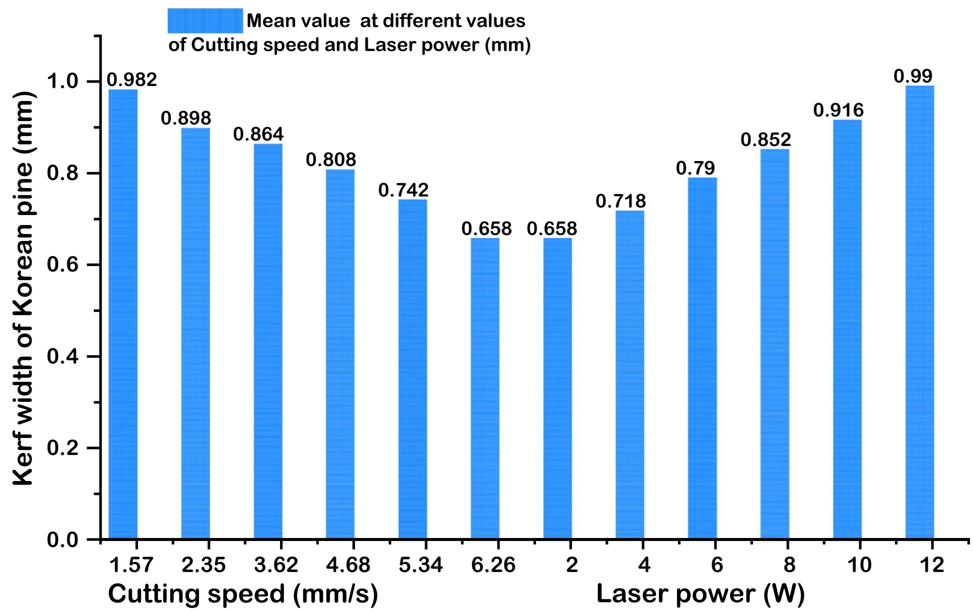

Fig. 18 Illustration of Korean pine kerf width under M_1 and M_2

Table 28 Cutting speed

	N	Mean	SD	SEM	Variance	Missing	Non-missing
S1.57	30	0.68367	0.1213	0.02215	0.01471	0	30
S2.35	30	0.68367	0.1213	0.02215	0.01471	0	30
S3.62	30	0.68367	0.1213	0.02215	0.01471	0	30
S4.68	30	0.68367	0.1213	0.02215	0.01471	0	30
S5.34	30	0.68367	0.1213	0.02215	0.01471	0	30
S6.26	30	0.68367	0.1213	0.02215	0.01471	0	30

Table 29 Laser power

	N	Mean	SD	SEM	Variance	Missing	Non-Missing
P2	30	0.534	0.01522	0.00278	2.31724E−4	0	30
P4	30	0.58	0.01438	0.00263	2.06897E−4	0	30
P6	30	0.622	0.01186	0.00217	1.4069E−4	0	30
P8	30	0.706	0.01886	0.00344	3.55862E−4	0	30
P10	30	0.792	0.02172	0.00397	4.71724E−4	0	30
P12	30	0.868	0.02905	0.0053	8.44138E−4	0	30

Table 30 Cutting speed & laser power interaction

		N	Mean	SD	SEM	Variance	Missing	Non–missing
S1.57	P2	5	0.534	0.01673	0.00748	2.8E−4	0	5
	P4	5	0.58	0.01581	0.00707	2.5E−4	0	5
	P6	5	0.622	0.01304	0.00583	1.7E−4	0	5
	P8	5	0.706	0.02074	0.00927	4.3E−4	0	5
	P10	5	0.792	0.02387	0.01068	5.7E−4	0	5
	P12	5	0.868	0.03194	0.01428	0.00102	0	5
S2.35	P2	5	0.534	0.01673	0.00748	2.8E−4	0	5
	P4	5	0.58	0.01581	0.00707	2.5E−4	0	5
	P6	5	0.622	0.01304	0.00583	1.7E−4	0	5
	P8	5	0.706	0.02074	0.00927	4.3E−4	0	5
	P10	5	0.792	0.02387	0.01068	5.7E−4	0	5
	P12	5	0.868	0.03194	0.01428	0.00102	0	5
S3.62	P2	5	0.534	0.01673	0.00748	2.8E−4	0	5
	P4	5	0.58	0.01581	0.00707	2.5E−4	0	5
	P6	5	0.622	0.01304	0.00583	1.7E−4	0	5
	P8	5	0.706	0.02074	0.00927	4.3E−4	0	5
	P10	5	0.792	0.02387	0.01068	5.7E−4	0	5
	P12	5	0.868	0.03194	0.01428	0.00102	0	5
S4.68	P2	5	0.534	0.01673	0.00748	2.8E−4	0	5
	P4	5	0.58	0.01581	0.00707	2.5E−4	0	5
	P6	5	0.622	0.01304	0.00583	1.7E−4	0	5
	P8	5	0.706	0.02074	0.00927	4.3E−4	0	5
	P10	5	0.792	0.02387	0.01068	5.7E−4	0	5
	P12	5	0.868	0.03194	0.01428	0.00102	0	5
S5.34	P2	5	0.534	0.01673	0.00748	2.8E−4	0	5
	P4	5	0.58	0.01581	0.00707	2.5E−4	0	5
	P6	5	0.622	0.01304	0.00583	1.7E−4	0	5
	P8	5	0.706	0.02074	0.00927	4.3E−4	0	5
	P10	5	0.792	0.02387	0.01068	5.7E−4	0	5
	P12	5	0.868	0.03194	0.01428	0.00102	0	5
S6.26	P2	5	0.534	0.01673	0.00748	2.8E−4	0	5
	P4	5	0.58	0.01581	0.00707	2.5E−4	0	5
	P6	5	0.622	0.01304	0.00583	1.7E−4	0	5
	P8	5	0.706	0.02074	0.00927	4.3E−4	0	5
	P10	5	0.792	0.02387	0.01068	5.7E−4	0	5
	P12	5	0.868	0.03194	0.01428	0.00102	0	5

Table 31 Overall ANOVA results

	DF	Sum of squares	Mean square	*F* value	*P* value
Cutting speed	5	−4.16334E−17	−8.32667E−18	−1.83677E−14	–
Laser power	5	2.4949	0.49898	1100.69118	8.42696E−113
Interaction	25	0	0	0	1
Model	35	2.4949	0.07128	157.2416	4.06372E−98
Error	144	0.06528	4.53333E−4		
Corrected Total	179	2.56018			

Table 32 Cutting speed and laser power

Cutting speed	Mean	Groups	Laser power	Mean	Groups					
S1.57	0.68367	A	P12	0.868	A					
S2.35	0.68367	A	P10	0.792		B				
S3.62	0.68367	A	P8	0.706			C			
S4.68	0.68367	A	P6	0.622				D		
S5.34	0.68367	A	P4	0.58					E	
S6.26	0.68367	A	P2	0.534						F

Table 33 Cutting speed & laser power interaction

Cutting speed	Laser power	Mean	Groups				
S6.26	P12	0.868	A				
S5.34	P12	0.868	A				
S4.68	P12	0.868	A				
S3.62	P12	0.868	A				
S2.35	P12	0.868	A				
S1.57	P12	0.868	A				
S6.26	P10	0.792		B			
S5.34	P10	0.792		B			
S1.57	P10	0.792		B			
S4.68	P10	0.792		B			
S2.35	P10	0.792		B			
S3.62	P10	0.792		B			
S5.34	P8	0.706			C		
S3.62	P8	0.706			C		
S4.68	P8	0.706			C		
S6.26	P8	0.706			C		
S1.57	P8	0.706			C		
S2.35	P8	0.706			C		
S5.34	P6	0.622				D	
S3.62	P6	0.622				D	
S6.26	P6	0.622				D	
S2.35	P6	0.622				D	
S4.68	P6	0.622				D	
S1.57	P6	0.622				D	
S6.26	P4	0.58				D	E
S4.68	P4	0.58				D	E
S3.62	P4	0.58				D	E
S5.34	P4	0.58				D	E
S2.35	P4	0.58				D	E
S1.57	P4	0.58				D	E
S6.26	P2	0.534					E
S5.34	P2	0.534					E
S2.35	P2	0.534					E
S4.68	P2	0.534					E
S3.62	P2	0.534					E
S1.57	P2	0.534					E

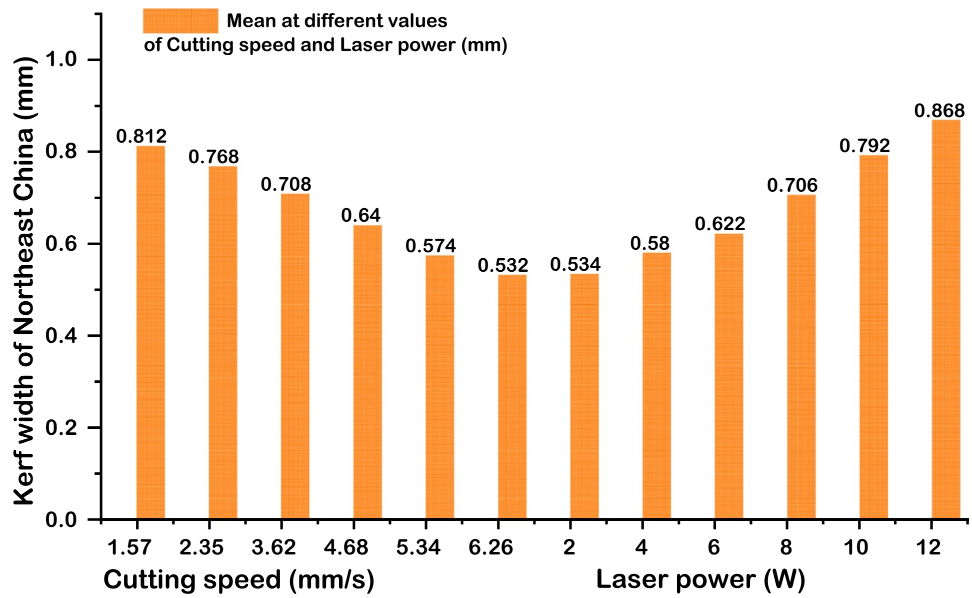

Fig. 19 Illustration of Northeast China ash kerf width under M_1 and M_2

3. The Korean pine was most affected during WJGL machining under different laser cutting speeds and powers. Its kerf width variations were significant compared to the Northeast China ash. Besides, the WJGL power was the most influenced parameter, followed by cutting speed in terms of kerf width, geometry, and surface quality. Moreover, the interaction between the cutting speed and laser power was significant for Korean pinewood and not significant for Northeast China ashwood.

Acknowledgements The authors are thankful to the Forestry and Woodworking Machinery Engineering Technology Center of the Northeast Forestry University for the machining facility and the College of Mechanical and Electrical Engineering members.

Author Contributions All authors contributed to the study's design and conceptualization and agreed on the final version of the manuscript. DBS carried out methodology, software, formal analysis, and the original draft preparation; the validation by YC, LJ, and MY; resources by MY and YC; data curation by DBS, LQ, and QW; writing-review and editing by LJ, LQ, and QW; supervision and funding acquisition by YC.

Funding This study was funded by Major Special Research and Development Projects in Guangdong Province (2020B020216001), Fundamental Research for the Central Universities (2572019CP18).

Data availability The supplementary supporting data is publicly available at: https://data.mendeley.com/datasets/gj5bxpsyvg/1

Code availability There is no code available for this work.

Declaration

Conflict of interest The authors have no financial or proprietary interests in any material discussed in this article.

References

1. Pocorni J, Han SW, Cheon J et al (2017) Numerical simulation of laser ablation driven melt waves. J Manuf Process 30:303–312. https://doi.org/10.1016/j.jmapro.2017.09.032
2. Choudhury IA, Shirley S (2010) Laser cutting of polymeric materials: an experimental investigation. Opt Laser Technol 42:503–508. https://doi.org/10.1016/J.OPTLASTEC.2009.09.006
3. Tahir BA, Ahmed R, Ashiq MGB et al (2012) Cutting of nonmetallic materials using Nd:YAG laser beam. Chinese Phys B 21:44201. https://doi.org/10.1088/1674-1056/21/4/044201
4. Powell J, Kaplan A (2004) Laser cutting: From first principles to the state of the art. In: Brandt M, Harvey E (eds) 1st Pacific international conference on application of lasers and optics, p 6
5. Doumbia BS, Yang C, Ma Y, et al (2021) Analysis of neodymium-doped yttrium-aluminum-garnet laser and experimental prospects for cutting micro-thin black walnut veneers in industry. BioResources 16:2416–2432. https://doi.org/10.15376/biores.16.2.2416-2432

6. Islam MN, Ando K, Yamauchi H et al (2007) Passive impregnation of liquid in impermeable lumber incised by laser. J Wood Sci 53:436–441. https://doi.org/10.1007/s10086-006-0878-0
7. Powell J (1998) CO2 Laser cutting, 2nd edn. Springer-Verlag, London Limited
8. Listyanto T, Ando K, Yamauchi H, Hattori N (2013) Microwave and steam injection drying of CO2 laser incised Sugi lumber. J Wood Sci 59:282–289. https://doi.org/10.1007/s10086-013-1331-9
9. Schuocker D (1989) Laser cutting. Mater Manuf Process 4:311–330. https://doi.org/10.1080/10426918908956297
10. Guillas C, Le C, Theveney S, Lefebvre P (1990) Comparative performances of C02 and YAG lasers in the cutting of stainless steel. SPIE 1277:244–255
11. Fork RL, Schehrer KL, Hirlimann C et al (1989) Amplification of femtosecond optical pulses using a double confocal resonator. Opt Lett 14:1068. https://doi.org/10.1364/ol.14.001068
12. Fukuta S, Nomura M, Ikeda T et al (2016) Wavelength dependence of machining performance in UV-, VIS- and NIR-laser cutting of wood. J Wood Sci 62:316–323. https://doi.org/10.1007/s10086-016-1553-8
13. Olsen FO, Alting L (1995) Pulsed laser materials processing, ND-YAG versus CO2 lasers. CIRP Ann Manuf Technol 44:141–145. https://doi.org/10.1016/S0007-8506(07)62293-8
14. Zhu M, Hall JL (1997) Atomic, molecular, and optical physics: electromagnetic radiation, experiment. Academic Press Limited, London
15. Trumpf (2007) Technical information laser processing: CO2 laser. TRUMPF Werkzeugmaschinen GmbH + Co. KG. https://docplayer.net/27024582-Technical-information-laser-processing.html
16. Gong Y (2014) An on-line learning and training tool for laser cutting. Master Dissertation, University of Manchester. http://www.manchester.ac.uk/escholar/uk-ac-man-scw:247478
17. Wang Z (2012) An investigation on water jet machining for hardwood floors. Eur J Wood Wood Prod 70:55–59. https://doi.org/10.1007/s00107-010-0492-0
18. Kilchling P, Hansmann R, Seeland K (2009) Demand for non-timber forest products: Surveys of urban consumers and sellers in Switzerland. For Policy Econ 11:294–300. https://doi.org/10.1016/j.forpol.2009.05.003
19. Yang C, Lu Y, Ma Y, et al (2017) Theoretical and experimental study on the cutting of wood by nanosecond pulse laser. Linye Kexue/Scientia Silvae Sin 53:151–156. https://doi.org/10.11707/j.1001-7488.20170918
20. Jiang X, Li J, Bai Y et al (2016) Laser cutting wood test and influencing factors of processing quality. Laser Optoelectron Prog 53:031403. https://doi.org/10.3788/lop53.031403
21. Li Jinzhe (2016) Microscopic analysis and experimental study of laser processing quality of wood. Northeast Forestry University
22. Yang C, Deng Z, Li F, et al (2018) Design and experiment for a numerical control nanosecond water-jet-guided laser processing test bench. BioResources 13:6098–6109. https://doi.org/10.15376/biores.13.3.6098-6109
23. Jiang T, Yang C, Yu Y, et al (2021) Prediction and analysis of surface quality of Northeast China ash wood during water-jet assisted CO2 Laser Cutting. J Renew Mater 9:119–128. https://doi.org/10.32604/jrm.2021.011490
24. Tabie VM, Koranteng MO, Yunus A, Kuuyine F (2019) Water-jet guided laser cutting technology—an overview. Lasers Manuf Mater Process 6:189–203. https://doi.org/10.1007/s40516-019-00089-9
25. Tangwarodomnukun V, Wang J, Huang CZ, Zhu HT (2012) An investigation of hybrid laser waterjet ablation of silicon substrates. Int J Mach Tools Manuf 56:39–49. https://doi.org/10.1016/j.ijmachtools.2012.01.002
26. Yang C, Jiang T, Yu Y, et al (2018) Study on surface quality of wood processed by water-jet assisted nanosecond laser. BioResources 13:3125–3134. https://doi.org/10.15376/biores.13.2.3125-3134
27. Yang C, Jiang T, Yu Y et al (2019) Waterjet assisted nanosecond laser microcutting of Northeast China ash wood: experimental study. BioResources 14:128–138. https://doi.org/10.15376/biores.14.1.128-138
28. Rajendran N (1990) An experimental and theoretical study of heat transfer effects during a laser-cutting process. Doctoral Dissertation, Iowa State University. https://lib.dr.iastate.edu/rtd/9407/
29. Zhou BH, Mahdavian SM (2004) Experimental and theoretical analyses of cutting nonmetallic materials by low power CO2-laser. J Mater Process Technol 146:188–192. https://doi.org/10.1016/j.jmatprotec.2003.10.017
30. Pocorni J (2017) Laser Cutting and Piercing: Experimental and Theoretical Investigation. Doctoral Dissertation, Lulea University of Technology. https://www.researchgate.net/publication/346037036
31. Powell J, Kaplan A (2004) Laser cutting: from first principles to the state of the art. In: Pacific international conference on applications of lasers and optics. Laser Institute of America, Melbourne Australia, pp 1–6
32. Vago N, Pavius M, Lee K et al (2009) Advanced micromachining combining nanosecond lasers with water jet-guided laser technology. Laser Appl Microelectron Optoelectron Manuf VII 7201:72010A. https://doi.org/10.1117/12.814712
33. Li L, Wang Y, Yang L, Chu J (2007) Experimental research on waterjet guided laser processing. In: Kulchin YN, Ou J, Vitrik OB, Zhou Z (eds) Proceedings of SPIE, p 6
34. Kruusing A (2004) Underwater and water-assisted laser processing: Part 1—general features, steam cleaning and shock processing. Opt Lasers Eng 41:307–327. https://doi.org/10.1016/S0143-8166(02)00142-2
35. Kruusing A (2008) Handbook of liquids-assisted laser processing, 1st edn. Elsevier
36. Wagner FR, Spiegel A, Vago N, Richerzhagen B (2002) Water-jet guided laser: possibilities and potential for singulation of electronic packages. Phot Process Microelectron Photonics 4637:479. https://doi.org/10.1117/12.470656
37. Perrottet D, Spiegel A, Amorosi S, Richerzhagen B (2005) GaAs-wafer dicing using the water jet guided laser. In: 2005 International Conference on Compound Semiconductor Manufacturing Technology. Synova SA, Ch. De la Dent-d'Oche, 1024 Ecublens, Switzerland, New Orleans, LA(US), p 4
38. Gabzdyl JT (1989) The effect of laser mode and coaxial gas jet on laser cutting. Doctoral Dissertation, Imperial College London (University of London). http://ethos.bl.uk/OrderDetails.do?uin=uk.bl.ethos.266851
39. Wang Y, Ando K, Hattori N (2013) Changes in the anatomy of surface and liquid uptake of wood after laser incising. Wood Sci Technol 47:447–455. https://doi.org/10.1007/s00226-012-0497-4
40. Ming Y, Shuang S, Shi-hui J, et al (2015) Theory research of wood surface cells explosion heated by nanosecond laser. For Mach Woodwork Equip, pp 2–4. https://doi.org/10.13279/j.cnki.fmwe.2015.0026
41. Panzner M, Wiedemann G, Henneberg K et al (1998) Experimental investigation of the laser ablation process on wood surfaces. Appl Surf Sci 127–129:787–792. https://doi.org/10.1016/S0169-4332(97)00743-5
42. Yang C, Liu Q, Li X et al (2019) Theoretical process parameter calculation and test verification of laser cutting veneer. Sci Silvae Sin (Linye Kexue) 55:173–180. https://doi.org/10.11707/j.1001-7488.20191218

43. Leone C, Pagano N, Lopresto V, Iorio I De (2009) Solid state Nd:YAG laser cutting of CFRP sheet: influence of process parameters on kerf geometry and HAZ. In: The 17th International Conference on Composite Materials. pp 1–10
44. Doumbia BS, Chunmei Y, Yan M, et al (2021) Practical analysis of nanosecond water-jet guided laserwood machining. Mendeley Data V2:1–36. https://doi.org/10.17632/gj5bxpsyvg.1